Closed-form design formulae for seismically isolated structure with a damping enhanced inerter system

Chao Pan [1], Jieling Jiang [2,3], Ruifu Zhang [2,3 *], Yuying Xia [4]

[1] College of Civil Engineering, Yantai University, Yantai 264005, China
[2] State Key Laboratory of Disaster Reduction in Civil Engineering, Tongji University, Shanghai 200092, China
[3] Department of Disaster Mitigation for Structures, Tongji University, Shanghai 200092, China
[4] College of Engineering, Swansea University, Fabian Way, Swansea, SA1 8EN, UK

Abstract

Existing studies mainly focused on the mass enhancement effect of the inerter system within a seismically isolated structure. In this study, a new analytical perspective is introduced based on another attractive feature of the inerter system, namely, the damping enhancement effect. Accordingly, a ready-to-use optimal design method for isolated structure with the inerter system is proposed. First, the damping enhancement equation of the inerter system is reformulated in the form of equivalent damping ratio. Then, the closed-form design formulae of the inerter system is derived based on damping enhancement maximization and seismic demand. By taking the performance of both the primary structure and the isolation layer into consideration, the dual-target-oriented design strategy of the isolated structure is subsequently developed. And the closed-form design formulae of the inerter system is then integrated into the strategy to produce a practical design method for isolated structure with the inerter system. A seven-story isolated benchmark model is finally employed as the design case to exemplify the effectiveness of the proposed design method. Compared to the directly installed viscous damper case, structural base shear force, inter-story drift angle and the deformation of the isolation layer are more effectively reduced with the addition of the inerter system, and the energy dissipation capacity of the damper within the inerter system is improved substantially. Furthermore, the derived closed-form design formulae reduce the iterative calculation and bring high-efficient design for isolated structure with the inerter system.

Keywords: inerter system, base isolation, damping enhancement effect, closed-form design formulae, dual-target-oriented design strategy

1. Introduction

Base isolation technology has been extensively used in earthquake-prone regions to protect the structures from earthquake-induced damage [1, 2]. The principle of this technology is to transfer most of the seismic energy to the isolation system, such that the primary structure is almost decoupled from the ground motion and behaves similar to a rigid body. However, in doing this, a relative large displacement concentrates at the isolation layer, which may occupy a huge space for installation and cause inconvenience to the connection of utilities (gas and water supply system) [3]. As a consequence, a series of hybrid isolation systems are proposed by combining the traditional isolation system with passive vibration control devices [4-6]. Previous studies have investigated the effect of tuned mass dampers on base-isolated structures [7, 8]. Based on a similar principle as a tuned mass damper, some studies have also considered the use of a tuned liquid damper [9, 10] and a tuned liquid column damper [11, 12]. However, the effectiveness and application of these devices may be limited by the physical

mass that can be added to the primary structure [13].

As a more effective alternative, the idea of employing the inerter to base isolation system has attracted extensive attention recent years. Different from the traditional one-terminal mass element, the inerter is a two-terminal inertia mass element in which the inertial force is proportional to the relative acceleration between its two terminals [14-16]; i.e., $F_{in} = m_{in}(\ddot{u}_2 - \ddot{u}_1)$, where F_{in} is the inertial force of the inerter; m_{in} is the inertance with the dimension of mass, and $\ddot{u}_2 - \ddot{u}_1$ represents the relative acceleration across the two terminals. The two-terminal characteristic allows the apparent mass (inertance) to be far greater than the gravitational mass of the inerter without adding extra inertia force to the primary structure, which is the mass enhancement effect of the inerter system [16]. The specific realization of the two-terminal behavior can be achieved using the ball screw [16-18], hydraulic mechanism [19-21] and so forth [22-24], among which the ball-screw inerter has been applied in practical engineering structures [18, 25]. The ball screw inerter transfers the relative linear motion between the two terminals into the high-speed rotational motion of the flywheel, yielding large inertial force and viscous damping force [16]. In 1973, Kawamata [14] proposed a liquid mass pump, which was the early implementation of the two-terminal inertial element in civil engineering. Toward the end of the last century and the beginning of this century, Saito et al [26] and Ikago et al [16, 27] developed the tuned viscous mass damper, which explicitly used the mass enhancement effect and damping enhancement effect for the first time. However, the in-depth mechanism of the damping enhancement effect remained undiscovered at that time. Subsequently, Zhang et al [28] discovered the damping enhancement equation, which explains the theoretical essence of the damping enhancement effect in the perspective of the stochastic mean-square responses. Mass enhancement effect [16] and damping enhancement effect [16, 28] are the main advantages of the inerter system. In this regard, various inerter-based isolation systems have been proposed in the literature and have been termed as a gyro-mass damper [22, 29], a parallel inerter system [30-32], a serial inerter system [33] and a tuned inerter damper [34].

In addition to the development of inerter-based isolation devices, various optimization methods for the inerter-based isolated structure have also been investigated. Based on the H_2 design criteria, Qian et al [35] optimized the design parameters of the serial and parallel tuned inerter damper system by minimizing the root-mean-square responses. Li et al [36] obtained the parameters of the proposed clutching inerter damper system through H_2-based optimization, and found that clutching inerter damper system could realize less seismic energy input to the primary structure compared to the traditional base isolation system, but the optimal method based on this phenomenon remained undiscovered. De Domenico et al [37] conducted a systematic study of inerter-based isolation systems, in which the parameters were both obtained numerically by minimizing the displacement, acceleration or energy-based variances. Di Matteo et al [38] derived a simplified analytical solution to obtain the parameters of the tuned mass damper inerter to maximally reduce the displacement of the isolation layer and its control effectiveness was further assessed in [39]. De Angelis et al [40] determined the optimal parameters of the tuned mass damper inerter numerically through the energy-based optimization, but the primary concern was about the displacement and acceleration reductions. Zhao et al [41] developed a displacement-demand equation and on this basis proposed the isolation layer's

displacement-oriented optimal design method. As summarized above, the analytical solutions and numerical optimizations for isolated structures equipped with the inerter systems have been investigated. However, these studies have mainly focused on the mass enhancement effect or the vibration mitigation effect of the inerter system and on this basis propose a series of design method to optimize the performance of the primary structure or the isolation layer. Although the energy dissipation characteristic (less seismic energy input and more energy dissipation) of the inerter-based isolation system was mentioned in [36]. But an optimal design method explicitly using the damping enhancement effect of the inerter system in the isolated structures remains unexplored. Furthermore, the developed numerical design method is usually computationally expensive and not easy to implement in practical applications.

Therefore, in this study, a direct and ready-to-use optimal design method for isolated structure with the inerter system is proposed. First, stochastic responses of a single-degree-of-freedom (SDOF) structure with an inerter system is derived through random vibration analysis, and the damping enhancement equation of the inerter system is reformulated in the form of equivalent damping ratio. Then, the closed-form design formulae of the inerter system is derived based on the damping enhancement maximization and seismic demand. Based on the defined equivalent damping ratio, the relationship between the closed-form design formulae and the design spectrum is established. The dual-target-oriented design strategy of the isolated structure with the inerter system is subsequently developed, in which the seismic action mitigation ratio and deformation threshold of the isolation layer are adopted as the corresponding performance indicators. Finally, a seven-story isolated benchmark model is adopted as the design case, and time history analyses are carried out to exemplify the feasibility and effectiveness of the closed-form design formulae and the dual-target-oriented design strategy.

2. Theoretical basis

2.1 Mechanical model

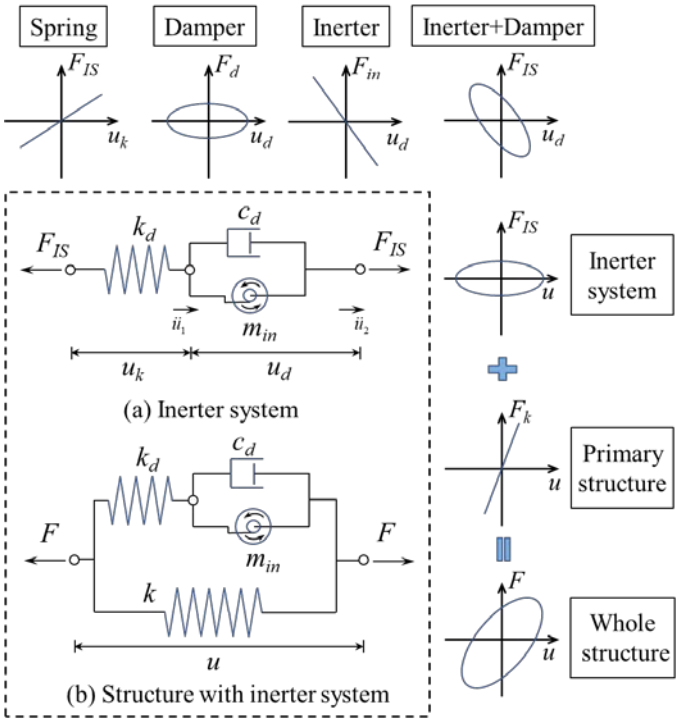

FIGURE 1 Diagram of the structure with inerter system and the corresponding force-deformation relationships

As shown in FIGURE 1 (a), the inerter system considered in this study comprises three mechanical elements: an inerter and a damper ~~are~~ mounted in parallel and then in series with the spring [16, 42], which has been adopted for analysis by many researchers in many independent studies [16, 41] and has been applied in practical engineering structures [25, 43]. The resisting force of the inerter system can be expressed by

$$F_{IS} = k_d u_k = m_{in}\ddot{u}_d + c_d\dot{u}_d \tag{1}$$

where $\ddot{u}_d$ and $\dot{u}_d$ are the relative acceleration and relative velocity of the inerter or the damper, respectively; u_k is the relative displacement of the serial spring; m_{in}, c_d, and k_d represent the inertance of the inerter, damping coefficient of the damper, and the stiffness of the spring, respectively.

Considering that the ~~essential concern~~main forcus of this study is the derivation of the closed form design formulae of the inerter system based on damping enhancement maximization and seismic demand, the mechanical behavior of the primary structure is assumed to be within the linear state. And the damper is simulated by the linear viscous damping element. The force-displacement relationships of each mechanical element are ~~along~~ shown in FIGURE 1. From the perspective of the force-displacement relationship, the inerter is characterized by negative stiffness [44-46], while the serial spring exhibits positive stiffness. Owing to the asynchronous vibration between the serial inerter and spring, the damping enhancement effect of the inerter system can be generated [16, 28]. ~~That is to say~~In other words, the deformation of the damper in the inerter system can be amplified by the inner actions between the inerter with negative stiffness and the serial spring with positive stiffness. Therefore, the energy dissipation efficiency of the damper in the inerter system can be immensely improved compared with the pure damper within the traditional isolation system under the same structural displacement. In other words, under the same input of seismic energy, the additional damping required within the inerter system can be smaller than the damping required in the device which relies on the pure damper to dissipate energy. The damping enhancement effect of the inerter system sets up the foundation of the closed-form design formulae of the inerter system being discussed in a later section.

2.2 Stochastic response solutions

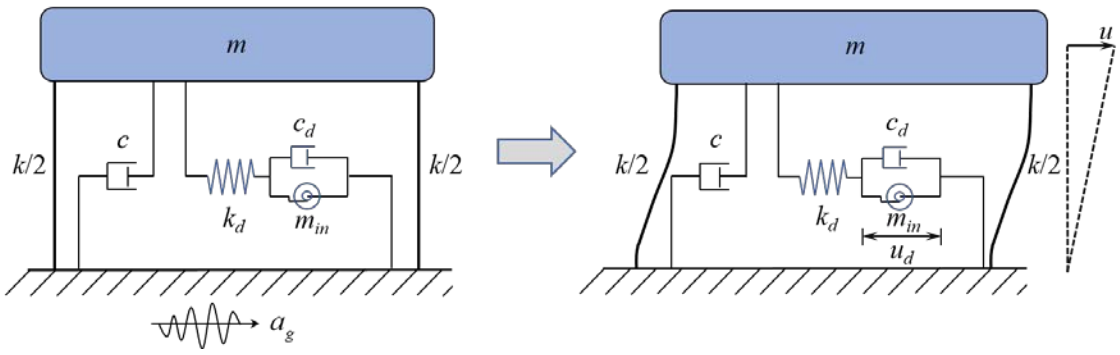

FIGURE 2 Analytical model of a SDOF structure with an inerter system

FIGURE 2 is the schematic diagram of the SDOF structure with an inerter system. According to the dynamic equilibrium conditions, the governing equations of motion can be established as follows

$$\begin{cases} m\ddot{u} + c\dot{u} + ku + k_d\left(u - u_d\right) = -ma_g \\ m_{in}\ddot{u}_d + c_d\dot{u}_d - k_d\left(u - u_d\right) = 0 \end{cases} \tag{2}$$

where u and u_d being the displacement of the primary structure and the two-terminal deformation of the inerter, respectively; m, c, k are the mass, damping coefficient and stiffness of the primary structure, respectively; and a_g is the acceleration of the input ground motion.

The following dimensionless parameters are introduced

$$\omega_0 = \sqrt{\frac{k}{m}} \qquad \zeta = \frac{c}{2m\omega_0} \qquad \mu = \frac{m_{in}}{m} \qquad \kappa = \frac{k_d}{k} \qquad \xi = \frac{c_d}{2m\omega_0} \tag{3}$$

where ω_0 and ζ are the circular frequency and inherent damping ratio of the primary structure, respectively; μ, κ, and ξ are the inertance-mass ratio, stiffness ratio and nominal damping ratio of the inerter system with respect to the primary structure, respectively.

Then, Equation (2) can be rewritten as

$$\begin{cases} \ddot{u} + 2\zeta\omega_0\dot{u} + \omega_0^2 u + \kappa\omega_0^2\left(u - u_d\right) = -a_g \\ \mu\ddot{u}_d + 2\xi\omega_0\dot{u}_d - \kappa\omega_0^2\left(u - u_d\right) = 0 \end{cases} \tag{4}$$

Assuming the input excitation is harmonic with a circular frequency of ω, Equation (4) can be transformed into the Laplace domain as follows

$$\begin{cases} s^2U + 2\zeta\omega_0 sU + \omega_0^2 U + \kappa\omega_0^2\left(U - U_d\right) = -A_g \\ \mu s^2 U_d + 2\xi\omega_0 sU_d - \kappa\omega_0^2\left(U - U_d\right) = 0 \end{cases} \tag{5}$$

where $s = i\omega$ with i represents the imaginary unit; U, U_d and A_g are the Laplace transformations of u, u_d and a_g, respectively.

By solving Equation (5), the transfer functions of u and u_d with respect to a_g can be given as follows

$$H_U(s) = \frac{U}{A_g} = \frac{-\left(s^2\mu + 2s\xi\omega_0 + \kappa\omega_0^2\right)}{s^4\mu + 2s^3\left(\zeta\mu + \xi\right)\omega_0 + s^2\left(\kappa + \mu + \kappa\mu + 4\zeta\xi\right)\omega_0^2 + 2s\left(\zeta\kappa + \xi + \kappa\xi\right)\omega_0^3 + \kappa\left(1+\mu\right)\omega_0^4} \tag{6}$$

$$H_{U_d}(s) = \frac{U_d}{A_g} = \frac{-\kappa\omega_0^2}{s^4\mu + 2s^3\left(\zeta\mu + \xi\right)\omega_0 + s^2\left(\kappa + \mu + \kappa\mu + 4\zeta\xi\right)\omega_0^2 + 2s\left(\zeta\kappa + \xi + \kappa\xi\right)\omega_0^3 + \kappa\left(1+\mu\right)\omega_0^4} \tag{7}$$

Based on the theory of random vibration [47], the mean-square response of the controlled system

under the input power spectrum S_X can be calculated as

$$\sigma^2 = \int_{-\infty}^{\infty} \left|H(\mathrm{i}\omega)\right|^2 S_X \mathrm{d}\omega \tag{8}$$

From Equation (8) it can be found that the exponent of the transfer function $H(\mathrm{i}\omega)$ is two whereas the exponent of the input power spectrum S_X is one, which indicates that the mean-square response σ^2 is more sensitive to the variation of $H(\mathrm{i}\omega)$. Meanwhile, to deduce the closed-form design formulae of the inerter system in the following section and considering the types of input power spectrum S_X is not the essential concern of this study, S_X is assumed as a white noise excitation with amplitude of S_0.

By substituting Equation (6) and Equation (7) into Equation (8), the integral in Equation (8) can be derived into the closed-form rational functions as follows [48]

$$\sigma_u^2 = \frac{\pi S_0}{2\omega_0^3} \cdot \frac{4\zeta^2\kappa\mu\xi + \xi\left[\kappa^2 + \kappa\mu(\mu-2) + \mu^2 + 4\xi^2\right] + \zeta\left(\kappa^2\mu^2 + 4\kappa\xi^2 + 4\mu\xi^2\right)}{4\zeta^3\kappa\mu\xi + \kappa^2\xi^2 + \zeta^2\left[\kappa^2\mu^2 + 4\mu\xi^2 + 4\kappa(1+\mu)\xi^2\right] + \zeta\xi\left[\mu^2 + \kappa^2(1+\mu^2) + 4\xi^2 + 2\kappa\left(-\mu + \mu^2 + 2\xi^2\right)\right]} \tag{9}$$

$$\sigma_{u_d}^2 = \frac{\pi S_0}{2\omega_0^3} \cdot \frac{\kappa\left[\kappa\xi + 4\zeta^2\mu\xi + \zeta((1+\kappa)\mu^2 + 4\xi^2)\right]}{4\zeta^3\kappa\mu\xi + \kappa^2\xi^2 + \zeta^2\left[\kappa^2\mu^2 + 4\mu\xi^2 + 4\kappa(1+\mu)\xi^2\right] + \zeta\xi\left[\mu^2 + \kappa^2(1+\mu^2) + 4\xi^2 + 2\kappa\left(-\mu + \mu^2 + 2\xi^2\right)\right]} \tag{10}$$

For the isolated structure, the stiffness of the isolation layer is far less than the stiffness of the primary structure, ~~such that a relatively large displacement concentrates at the isolation layer and the primary structure behaves similar to a rigid body. That is to say,~~ which means the relative displacement of the primary structure is much smaller compared to the displacement of the isolation layer. On this basis, the energy dissipated by the inherent damping of the primary structure is ~~relative~~ limited (~~which can be further shown by~~further explanation can be found in the energy response curves depicted in Section 5.2), accordingly, ~~and~~ the inherent damping of the primary structure can be ignored and the damping of the isolated structure can be considered to be provided by the additional energy dissipation device. ~~Therefore, the inherent damping of the primary structure can be ignored.~~ Equation (9) and Equation (10) can therefore be simplified as

$$\sigma_u^2 = \frac{\pi S_0}{2\omega_0^3} \cdot \frac{\kappa^2 + \kappa\mu(\mu-2) + \mu^2 + 4\xi^2}{\kappa^2\xi} \tag{11}$$

$$\sigma_{u_d}^2 = \frac{\pi S_0}{2\omega_0^3\xi} \tag{12}$$

2.3 Damping enhancement equation formulated with the equivalent damping ratio

From Section 2.1, it can be known that the damping enhancement effect is one of the potential features of the inerter system. And the damping enhancement equation proposed in [28] was expressed in the form of the stochastic mean-square responses. In this subsection, the damping enhancement equation of the inerter system is formulated in another perspective, that is, derived from the equivalent

damping ratio. The damping enhancement equation of the inerter system can be expressed as [28]

$$\zeta + \lambda^2 \xi = \frac{1}{\tilde{\sigma}_u^2} \tag{13}$$

where $\tilde{\sigma}_u^2$ is the dimensionless form of σ_u^2 in Equation (11) by multiplying $\frac{2\omega_0^3}{\pi S_0}$; λ is the damping deformation enhancement ratio, which can be defined as follows

$$\lambda = \frac{\tilde{\sigma}_{u_d}}{\tilde{\sigma}_u} \tag{14}$$

where $\tilde{\sigma}_{u_d}$ is the dimensionless form of σ_{u_d} in Equation (12) by multiplying $\frac{2\omega_0^3}{\pi S_0}$.

Based on Equation (11) and Equation (12), λ can be further expressed as

$$\lambda^2 = \frac{\kappa^2}{\kappa^2 + \kappa\mu(\mu - 2) + \mu^2 + 4\xi^2} \tag{15}$$

For a SDOF structure with an equivalent damping ratio ζ_{eq}, the mean-square displacement response can be obtained [47]

$$\sigma_u^2 = \frac{\pi S_0}{2\omega_0^3 \zeta_{eq}} \tag{16}$$

Then ζ_{eq} can be expressed as

$$\zeta_{eq} = \frac{\pi S_0}{2\omega_0^3} \cdot \frac{1}{\sigma_u^2} = \frac{1}{\tilde{\sigma}_u^2} \tag{17}$$

Substituting Equation (17) into Equation (13) follows that

$$\zeta_{eq} = \zeta + \lambda^2 \xi \tag{18}$$

Therefore, Equation (18) is another formulation of the damping enhancement equation of the inerter system, that is, expressed with the equivalent damping ratio ζ_{eq}, which can be used to establish the relationship between the closed-form design formulae of the inerter system and the design spectrum (the relevant detail will be illustrated in the subsequent section). Assuming that the inherent damping of the primary structure is ignored, Equation (18) can be simplified as

$$\zeta_{eq} = \lambda^2 \xi \tag{19}$$

3. Closed-form design formulae of the inerter system

The appropriate selection of the parameters of the inerter system is an essential step during the optimal design process of isolated structure with the inerter system. Therefore, this section aims to derive closed-form design formulae of the inerter system based on the damping enhancement effect of the inerter system and seismic demand of the primary structure. Form Equation (18) it can be seen that the damping deformation enhancement ratio λ is inversely proportional to the nominal damping

ratio ξ with a pre-specified ζ_{eq} which correlates to the performance of the primary structure (will be illustrated in Section 4). In other words, in the condition that the target performance of the primary structure is satisfied, the damping enhancement effect of the inerter system can be maximized by minimizing the nominal damping ratio ξ of the inerter system. Therefore, the goal is to find the best set of the parameters that minimize ξ when the desired structural performance is pre-specified. Consequently, ξ is the objective function to be minimized. And the target equivalent damping ratio $\zeta_{eq,t}$ is selected as the constraint condition. Then, the design strategy can be transformed into an optimization problem as follows

$$\begin{aligned} &\underset{\mu,\xi,\kappa}{\text{minimize}} \quad \xi \\ &\text{subject to} \quad \zeta_{eq}(\mu,\xi,\kappa) = \zeta_{eq,t} \end{aligned} \tag{20}$$

where $\zeta_{eq,t}$ is the target equivalent damping ratio determined via performance demand of the primary structure.

The above optimization process can be solved using the Lagrange multiplier method [49] to find the minimum value of ξ under the constraint condition $\zeta_{eq}(\mu,\xi,\kappa) = \zeta_{eq,t}$. The Lagrange function can be established as follows

$$L(\mu,\kappa,\lambda) = \xi + \lambda\left[\zeta_{eq}(\mu,\xi,\kappa) - \zeta_{eq,t}\right] \tag{21}$$

where λ is the Lagrangian multiplier. The minimum of Lagrange function. $L(\mu,\kappa,\lambda)$. can be found by setting the partial derivatives of $L(\mu,\kappa,\lambda)$ with respect to the relevant variables to zeros, i.e.,

$$\frac{\partial L}{\partial \mu} = \frac{\partial \xi}{\partial \mu} + \lambda\frac{\partial \zeta_{eq}}{\partial \mu} = 0 \tag{22}$$

$$\frac{\partial L}{\partial \kappa} = \frac{\partial \xi}{\partial \kappa} + \lambda\frac{\partial \zeta_{eq}}{\partial \kappa} = 0 \tag{23}$$

$$\frac{\partial L}{\partial \lambda} = \zeta_{eq}(\mu,\xi,\kappa) - \zeta_{eq,t} = 0 \tag{24}$$

The following subsections are dedicated to illustrating the detailed derivations for determining the parameters of the inerter system based on the above optimization strategy.

3.1 Optimal stiffness ratio

Substituting Equation (19) into Equation (22) follows that

$$\frac{\partial L}{\partial \mu} = \left(\lambda + \frac{1}{\alpha^2}\right)\frac{\partial \zeta_{eq}}{\partial \mu} = 0 \tag{25}$$

If Equation (25) has a definite solution, the former part $\left(\lambda + \frac{1}{\alpha^2}\right)$ cannot be zero. Therefore, the

above equation is satisfied when the $\frac{\partial \zeta_{eq}}{\partial \mu}$ equals zero.

According to the differentiation of implicit function, substituting Equation (11) and Equation (17) into Equation (25) yields that

$$\frac{2\left[\kappa(\mu-1)+\mu\right]\kappa^2\xi}{\left[\kappa^2+\kappa(-2+\mu)\mu+\mu^2+4\xi^2\right]^2}=0 \tag{26}$$

Note that the nominal damping ratio ξ, the stiffness ratio κ and the denominator cannot be zero, therefore

$$\kappa(\mu-1)+\mu=0 \tag{27}$$

Then, the optimal stiffness ratio κ_{opt} is obtained

$$\kappa_{opt}=\frac{\mu}{1-\mu} \tag{28}$$

3.2 Optimal nominal damping ratio

Similarly, substituting Equation (19) into Equation (23) yields that

$$\frac{\partial L}{\partial \kappa}=\left(\lambda+\frac{1}{\alpha^2}\right)\frac{\partial \zeta_{eq}}{\partial \kappa}=0 \tag{29}$$

Likewise, the former part $\left(\lambda+\frac{1}{\alpha^2}\right)$ cannot be zero. Therefore, the above equation is satisfied when the $\frac{\partial \zeta_{eq}}{\partial \kappa}$ equals zero.

Similar in the above subsection, substituting Equation (11) and Equation (17) into Equation (29) takes the following form

$$\frac{\kappa\xi\left[\kappa(\mu-2)\mu+2\left(\mu^2+4\xi^2\right)\right]}{\left[\kappa^2+\kappa(-2+\mu)\mu+\mu^2+4\xi^2\right]^2}=0 \tag{30}$$

Note that ξ, κ and the denominator cannot be zero, therefore

$$\kappa(\mu-2)\mu+2\left(\mu^2+4\xi^2\right)=0 \tag{31}$$

Substitute Equation (28) into Equation (31), and the optimal nominal damping ratio ξ_{opt} can be obtained

$$\xi_{opt}=\frac{\mu}{2}\sqrt{\frac{\mu}{2(1-\mu)}} \tag{32}$$

Therefore, substituting Equation (28) and Equation (32) into Equation (15) leads to

$$\alpha^2=\frac{2}{(3-\mu)\mu} \tag{33}$$

4. Dual-target-oriented design strategy of isolated structure with the inerter system

4.1 Definition of the dual target

To achieve a highly efficient design, a dual-target-oriented design strategy is proposed in this section in which the performance of both the primary structure and the isolation layer are taken into consideration. The seismic action mitigation ratio β_h is defined to reflect the performance of the primary structure, and the deformation threshold of the isolation layer $[u_{iso}]$ is adopted as the performance indicator of the isolation layer. On the basis of the assumptions made in Section 2.1, the mechanical behavior of the isolation system is also assumed to be within the linear state to derive the practical design formulae of the isolated structure with inerter system in the subsequent section.

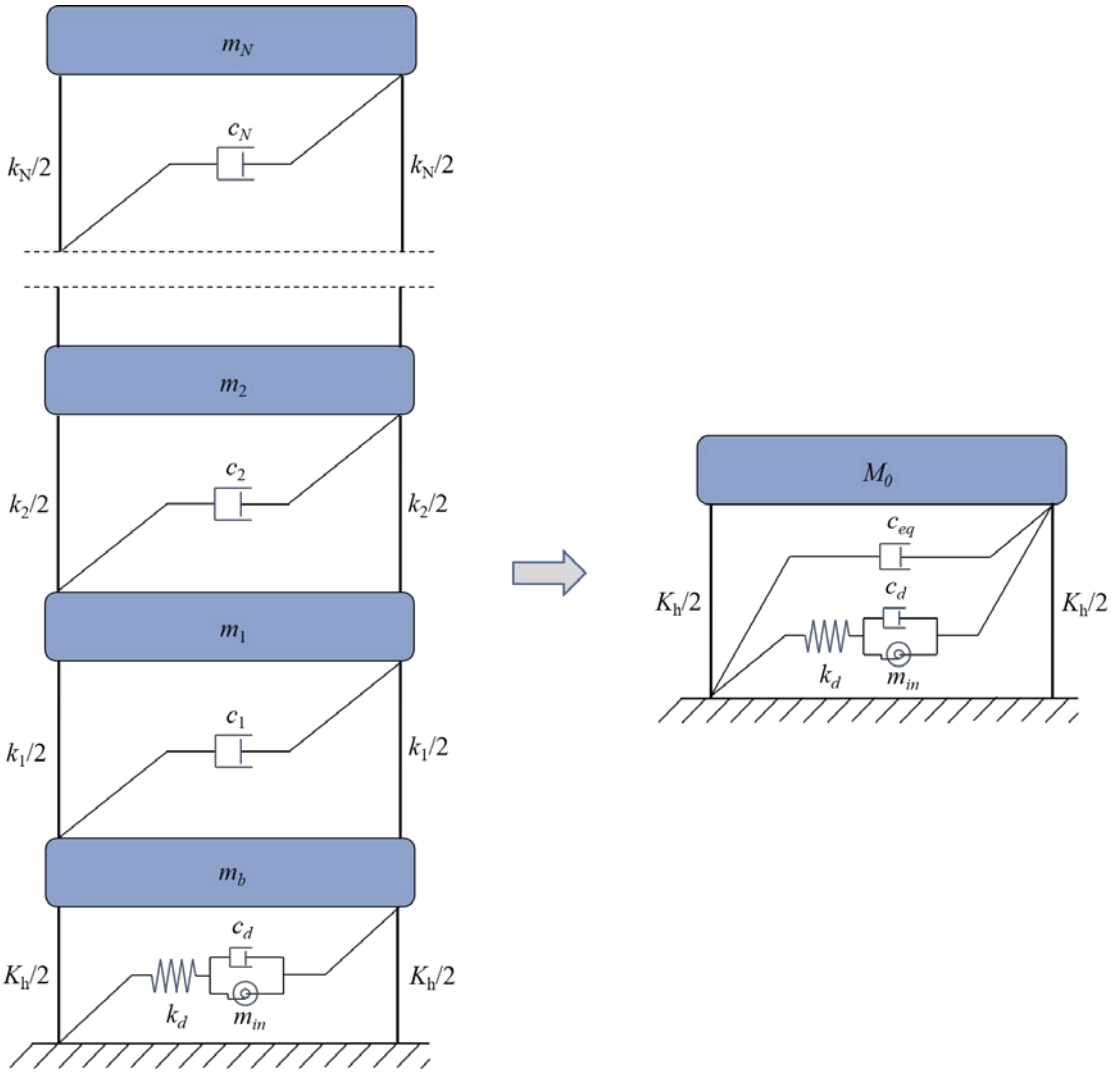

(a) MDOF model (b) SDOF model

FIGURE 3 Equalization of analysis model for isolated structure with the inerter system

For the isolated structure with the inerter system, the stiffness of the isolation layer is far less than

the stiffness of the primary structure, therefore the acceleration of the primary structure can be viewed as identical to those of the isolation layer. Consequently, as shown in FIGURE 3, the isolated structure with the inerter system is equivalent to a SDOF system with an equivalent damping coefficient c_{eq} (the reasonability of this equivalence will be further verified in Section 5). Then the seismic action can be expressed as [50]

$$F = M_0 S_a\left(T_b, \zeta_{eq,t}\right) \tag{34}$$

where M_0, $S_a\left(T_b, \zeta_{eq,t}\right)$, T_b, respectively, being the total mass, the acceleration spectrum, the isolation period of the isolated structure, respectively.

Assuming the original structure is within linear elastic state, the seismic action of the original structure (without additional isolation system) can be obtained [50]

$$F_0 = \chi M_0 S_a\left(T_0, \zeta\right) \tag{35}$$

where T_0 is the natural period of the original structure, and χ is the seismic action ratio of the original multi-story structure to the equivalent SDOF structure, which can be expressed as follows [51]

$$\chi \approx \frac{3\left(N+1\right)}{2\left(2N+1\right)} \tag{36}$$

where N is the story of the original structure. The detailed derivation process of Equation (36) is described in Appendix.

Based on Equation (34) and Equation (35), the seismic action mitigation ratio β_h can be defined

$$\beta_h = \frac{F}{F_0} = \frac{S_a\left(T_b, \zeta_{eq,t}\right)}{\chi S_a\left(T_0, \zeta\right)} \tag{37}$$

For the isolated structure, the deformation of the primary structure is mainly contributed by the isolation layer. Therefore, the deformation threshold of the isolation layer $[u_{iso}]$ can be expressed as follow

$$[u_{iso}] = S_d\left(T_b, \zeta_{eq,t}\right) \approx \frac{T_b^{\,2}}{4\pi^2} S_a\left(T_b, \zeta_{eq,t}\right) \tag{38}$$

in which S_a and S_d being the acceleration spectrum and displacement spectrum, respectively.

4.2 Practical design formulae

Based on Equation (37) and Equation (38), the isolation period T_b can be expressed by

$$T_b = 2\pi\sqrt{\frac{[u_{iso}]}{\chi\beta_h S_a\left(T_0, \zeta\right)}} \tag{39}$$

The stiffness of the isolation layer K_h can be then determined by

$$K_h = M_0 \left(\frac{2\pi}{T_b} \right)^2 \tag{40}$$

By substituting Equation (39) into Equation (37), $\zeta_{eq,t}$ can be obtained by solving the nonlinear equation using easy numerical methods. The details of this process are presented in Appendix. In this way, the closed-form design formulae obtained in Section 3 and the design spectrum shown in this section can be integrated together through $\zeta_{eq,t}$, thereby can produce a practical and highly efficient design method for the isolated structure with the inerter system.

Based on Equation (19), Equation (33) and Equation (32), $\zeta_{eq,t}$ can be further expressed as

$$\zeta_{eq,t} = \alpha^2 \xi_{opt} = \frac{1}{3-\mu} \sqrt{\frac{\mu}{2(1-\mu)}} \tag{41}$$

Therefore, based on Equation (41), μ can be obtained through the calculation process described in Appendix. The corresponding optimal κ_{opt} and ξ_{opt} can then be calculated based on Equation (28) and Equation (32).

Eventually, the parameters of the inerter system can be determined by

$$m_{in} = \mu \cdot M_0 \qquad k_d = \kappa_{opt} \cdot K_h \qquad c_d = 2\xi_{opt} \sqrt{M_0 \cdot K_h} \tag{42}$$

From the above procedure, parameters of the inerter system and the isolation layer can be both obtained. To verify the effectiveness of the proposed design method, time history analyses based on a benchmark model will be conducted in the next section (the seismic design code [52] requires that the performance of the isolated structures must be checked through time history analysis). Considering the assumptions made above (the isolated structure is equivalent to a SDOF system) and the numerical error between the spectrum analysis and time history analysis, the calculated indicators may not satisfy the target value well at the first calculation. Therefore, some adjustments need to be made accordingly based on the following principle: when β_h is not satisfied, ~~we decrease~~ the stiffness of the isolation layer K_h will be decreased to enhance the isolation effect so that the seismic action of the primary structure can be more effectively reduced. ~~However, w~~When u_{iso} exceeds the target value $[u_{iso}]$, ~~we mainly increase~~ the inertance-mass ratio μ will be increased accordingly to further enhance the role of the inerter system in controlling the excessive displacement concentrated in the isolation layer. The details of the whole design process are shown in the following flowchart.

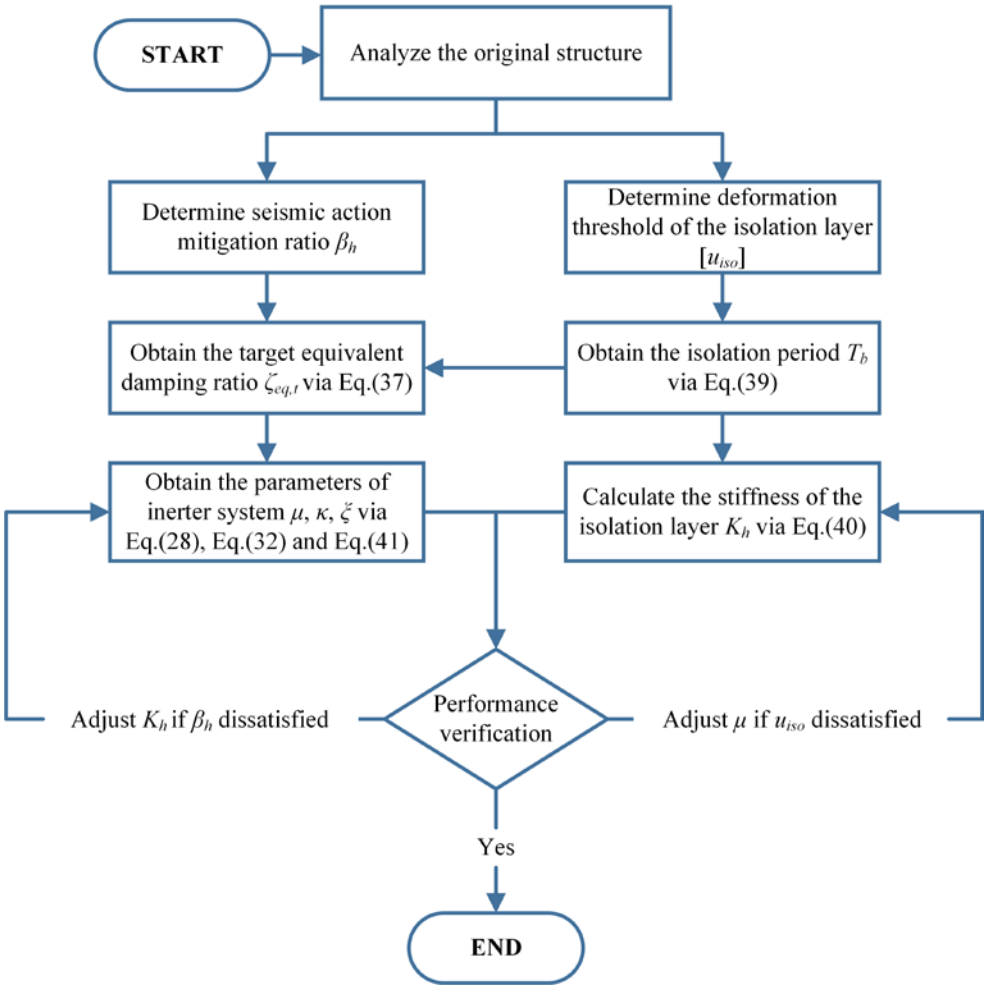

FIGURE 4 Flowchart of the dual-target-oriented design strategy of isolated structure with the inerter system

5. Case design

5.1 Parameter design

In this section, an isolated benchmark model [53] is adopted as the design case to verify the effectiveness of the proposed design method. TABLE 1 lists the details of the benchmark model. Additionally, the inherent damping ratio of the original structure is 2% and the mass of the isolation layer is 6115000 kg [53]. It is worth noting that the parameters of the equivalent SDOF model listed in Table 1 is based on the literature [53].

According to the initial analysis of the original structure, the dual target β_h and $[u_{iso}]$ are set to 0.4 and 360 mm, respectively. The acceleration spectrum value of the original structure $S_a(T_0,\zeta_0)$ can be calculated by the seismic design code [52]. Then T_b can be determined by Equation (39)

$$T_b = 2\pi\sqrt{\frac{[u_{iso}]}{\chi\beta_h S_a(T_0,\zeta_0)}} = 2\pi\times\sqrt{\frac{360\times10^{-3}}{0.8\times0.4\times0.559\times9.8}} = 2.846\ \text{s} \tag{43}$$

Then, the corresponding K_h can be calculated based on Equation (40)

$$K_h = M_0\left(\frac{2\pi}{T_b}\right)^2 = 27130\times\left(\frac{2\times\pi}{2.846}\right)^2\times10^3 = 1.322\times10^5\,\text{kN/m} \tag{44}$$

Subsequently, $\zeta_{eq,t}$ is obtained as 0.085 and μ is calculated as 0.108 through the practical iteration method illustrated in Appendix. The κ_{opt} and the ξ_{opt} can then be calculated by Equation (28) and Equation (32)

$$\kappa_{opt} = \frac{\mu}{1-\mu} = \frac{0.108}{1-0.108} = 0.121 \quad \xi_{opt} = \frac{\mu}{2}\sqrt{\frac{\mu}{2(1-\mu)}} = \frac{0.108}{2}\times\sqrt{\frac{0.108}{2\times(1-0.108)}} = 0.013 \tag{45}$$

The overall parameters of the inerter system and the isolation layer are summarized in TABLE 2.

5.2 Performance verification

Several time history analyses are carried out in this section based on the optimal parameters obtained in Section 5.1. It is worth noting that the original MDOF isolated model instead of the equivalent SDOF model is adopted in the time history analysis process to further verify the reasonability of the equivalence of the isolated structure with the inerter system illustrated in Section 4. Two artificial seismic waves (denoted as AW1 and AW2 in FIGURE 5) and five natural seismic waves (denoted as NW1-5 in FIGURE 5) are involved [52]: the artificial seismic waves are generated by the earthquake signal-processing tool EQSignal [54-57], and the natural seismic waves are downloaded from the PEER database center [58]. Detailed information of the natural seismic wave is listed in TABLE 3, and the normalized acceleration spectrum (the amplitude of all waves are adjusted to 1m/s) is shown in FIGURE 5.

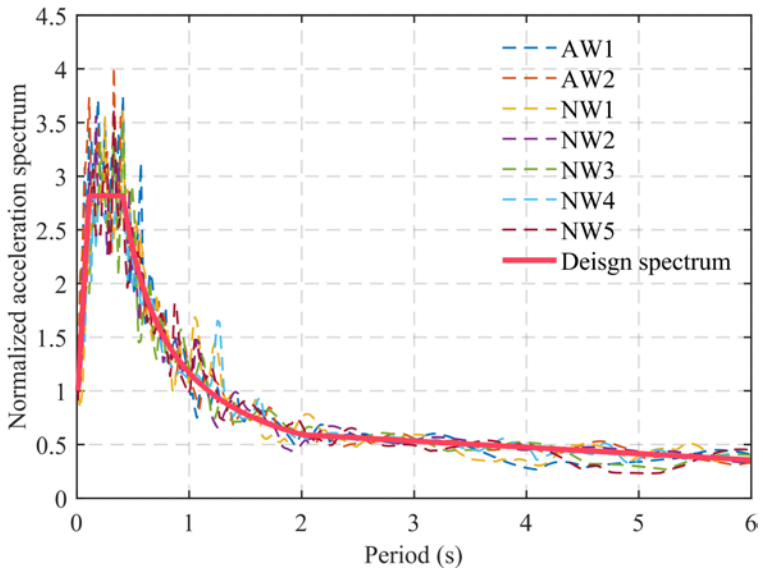

FIGURE 5 Normalized acceleration spectrum

To make the results comparable, the dynamic response of the isolated structure with the inerter system is compared with an isolated structure with viscous damper which the damping coefficient equals to c_d, and the amplitude of all the input excitations are adjusted to 0.4g [52]. TABLE 4 lists the seismic action mitigation ratio β_h and the deformation of the isolation layer u_{iso} under different input excitations and the average values are also calculated. It is shown that both the performance of the primary structure and the isolation layer satisfy the pre-specified target value, thereby confirming the reliability of the equivalent SDOF model adopted in Section 4 and the effectiveness of the proposed design method. FIGURE 6 and FIGURE 7 show the base shear force and deformation of the isolation layer under the El Centro wave (NW1), respectively. It can be observed that the base shear force is both effectively mitigated with the isolated structure equipped with the inerter system performs better than the viscous damper controlled case. Inspection of FIGURE 7, it can be also observed that the isolated structure equipped with the inerter system more effectively controls the deformation of the isolation layer. Considering AW1, NW1 and NW2 as examples, FIGURE 8 shows the structural inter-story drift angle of the original structure, the isolated structure equipped with viscous damper and equipped with the inerter system. The figures show that the inter-story drift angle is reduced with the addition of the inerter system, especially for the lower stories with larger story drift angles.

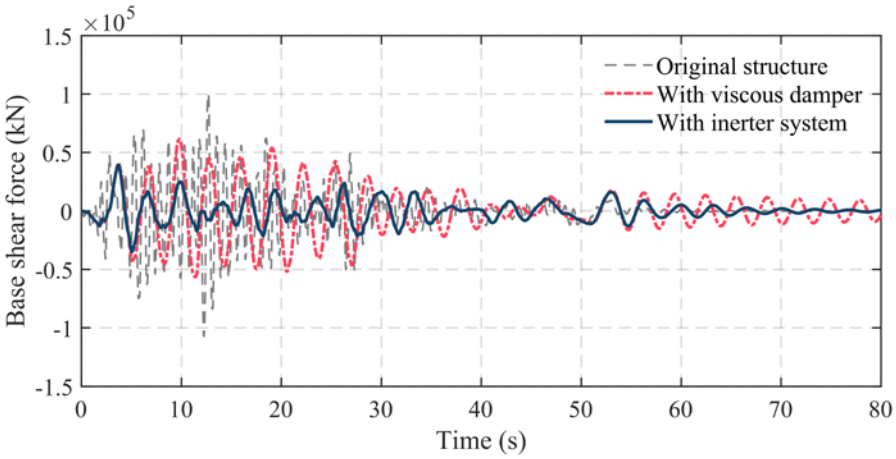

FIGURE 6 Base shear force responses under El Centro wave (NW1)

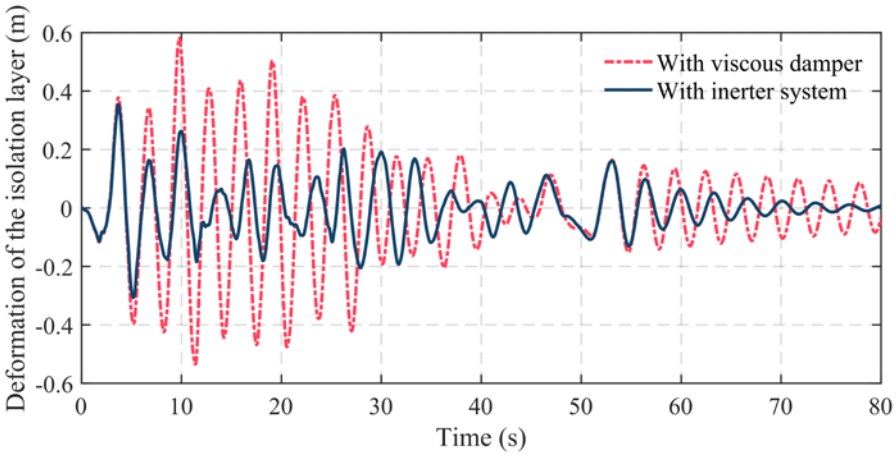

FIGURE 7 Deformation of the isolation layer in the isolated structure under El Centro wave (NW1)

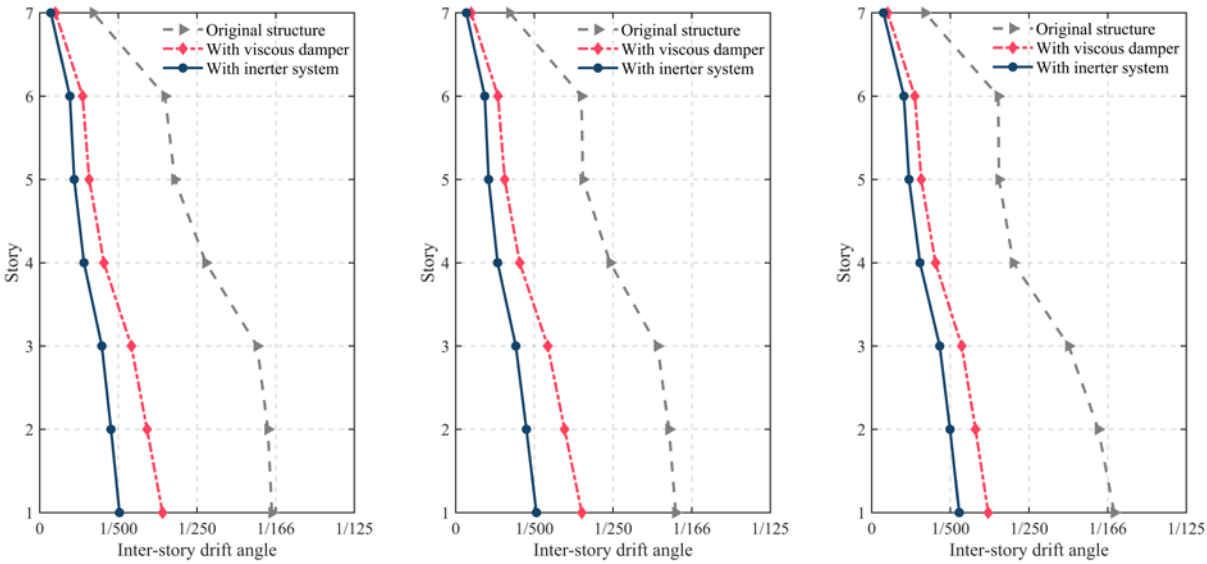

(a) AW1 (b) NW1 (c) NW2

FIGURE 8 Inter-story drift angle responses under different excitations

To present the damping enhancement effect of the inerter system, FIGURE 9 shows the hysteretic

curves of the viscous damper within the inerter system and the pure viscous damper under three excitations (AW1, NW1 and NW2). It is worth noting that the deformation and velocity of the viscous damper adopted here are equal to those of the isolation layer in the isolated structure with the inerter system to demonstrate the pure damping enhancement effect of the inerter system. From FIGURE 9, it can be clearly seen that the deformation and damping force of the damper in the inerter system are amplified and the energy dissipation efficiency are greatly improved compared to the pure viscous damper with the same damping coefficient, on the other hand demonstrating the effect of the damping enhancement maximization-based design brings. ~~Additionally, t~~The normalized energy response curves under NW1 are ~~also provided~~shown in FIGURE 10~~.~~, which illustrates ~~T~~the energy dissipated by the inherent damping of the primary structure are much smaller than by the damping of the isolated structure. This approves the ~~both small in FIGURE 10 (a) and (b), which further verify the~~ reasonability of ignoring the inherent damping of the primary structure discussed in Section 2.2. ~~From~~ FIGURE 10 (a) shows~~,~~ ~~–~~majority of the structural input energy is dissipated by the inerter system all the time, indicating a stable and efficient energy dissipation capacity of the inerter system. ~~From FIGURE 10 (b), t~~The energy dissipation of the pure viscous damper behaves not as effective as the inerter system in the early stage of the excitation, shown in FIGURE 10 (b)~~.~~

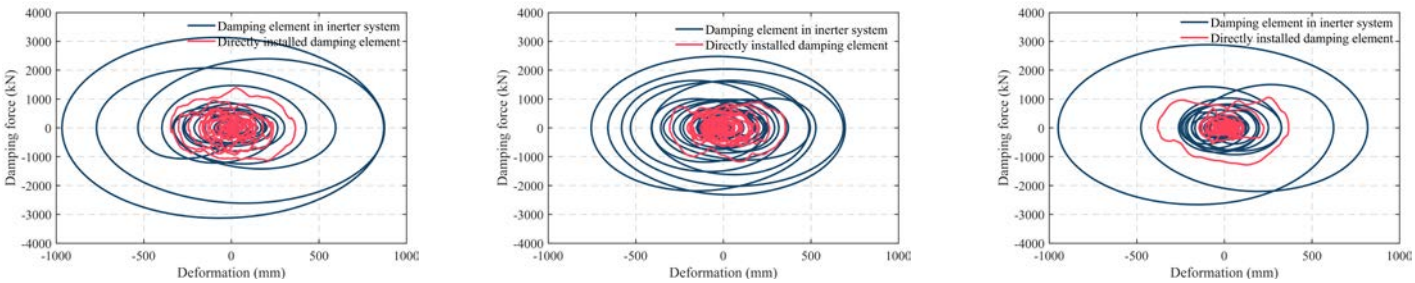

(a) AW1 (b) NW1 (c) NW2

FIGURE 9 Hysteretic curves of the damper under different excitations

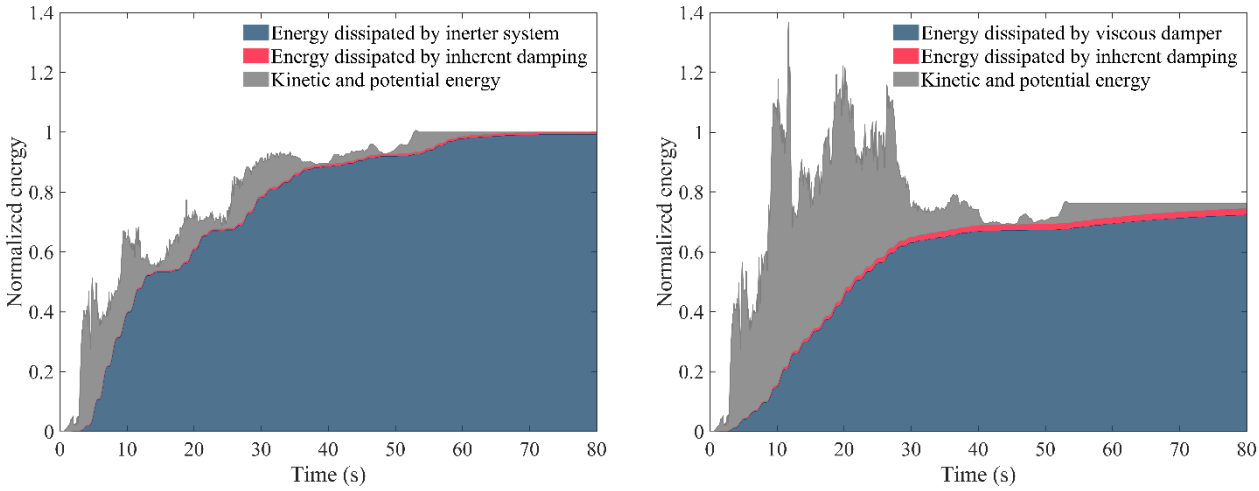

(a) Isolated structure with inerter system (b) Isolated structure with viscous damper

FIGURE 10 Normalized energy response curves of the isolated structure under NW1

6. Conclusions

A ready-to-use optimal design method for isolated structure with the inerter system is proposed in this study. The closform design formulae of the inerter system based on damping enhancement maximization and seismic demand is derived. The dual-target-oriented design strategy is then developed considering the performance of the primary structure and the isolation layer simultaneously. A seven-story isolated benchmark model with the inerter system is finally optimal designed and analyzed through time history analysis. The main conclusions are as follows:

(1) The damping enhancement equation of the inerter system is reformulated in the form of equivalent damping ratio. In addition, the equivalent damping ratio establishes the relationship between the derived closed-form design formulae of the inerter system and the design spectrum, thereby producing a practical design method for the isolated structure with the inerter system.

(2) The derived closed-form design formulae of the inerter system based on damping enhancement maximization and seismic demand yields a direct and simple way to design the parameters of the inerter system, which is beneficial for efficient design.

(3) The proposed dual-target-oriented design strategy considers both the performance of the primary structure and the isolation layer. Using the proposed optimal design method, structural base shear force, inter-story drift angle as well as the deformation of the isolation layer are more effectively controlled compared to the isolated structure equipped with pure viscous damper. Meanwhile, the energy dissipation capacity of the damper within the inerter system is improved substantially.

(4) The proposed optimal design method is straightforward and easy to implement and can reduce iterative calculation during the design process; thus, it is economically advantageous in terms of the computational cost.

(5) This study ~~analyzed merely~~focused on one type of inerter systems in the isolated structures. However, the principle of derivation of the closed-form design formulae and the dual-target-oriented design strategy ~~is not confined~~can be used for the applications of other types of inerter system. ~~to the application of the inerter system considered in this study~~. Further investigations will aim to ~~Other types of the inerter system with damping enhancement effect will be investigated in the future to generalize~~ extended the applicability of the proposed method with other types of inerter systems with damping enhancement effect. Additionally, it is promising for future study to extend the current work to the primary structure and the isolation system with nonlinear behavior.

7. Acknowledgements

This study was supported by the National Natural Science Foundation of China (grant no. 51978525 and 51778490), the Natural Science Foundation of Shandong Province, China (grant no. ZR2018BEE033), and the Foundation of Shanghai Science and Technology Commission (19DZ1202500).

8. References

[1] De Luca A, Guidi LG. State of art in the worldwide evolution of base isolation design. Soil Dynamics and Earthquake Engineering. 2019;125:13. https://doi.org/10.1016/j.soildyn.2019.105722

[2] Makris N. Seismic isolation: early history. Earthquake Engineering and Structural Dynamics. 2019;48:269-83. https://doi.org/10.1002/eqe.3124

[3] De Domenico D, Ricciardi G. An enhanced base isolation system equipped with optimal tuned mass damper inerter (TMDI). Earthquake Engineering and structural dynamics. 2018;47:1169-92. https://doi.org/10.1002/eqe.3011

[4] Ye K, Shu S, Hu L, Zhu HP. Analytical solution of seismic response of base-isolated structure with supplemental inerter. Earthquake Engineering and Structural Dynamics. 2019;48:1083-90. https://doi.org/10.1002/eqe.3165

[5] Xiang P, Nishitani A. Optimum design for more effective tuned mass damper system and its application to base-isolated buildings. Structural Control and Health Monitoring. 2014;21. https://doi.org/10.1002/stc.1556

[6] Li HT, Yang HT, Kwon IY, Ly FS. Bio-inspired passive base isolator with tuned mass damper inerter for structural control. Smart Materials and Structures. 2019;28:19. https://doi.org/10.1088/1361-665X/ab3239

[7] Taniguchi T, Der Kiureghian A, Melkumyan M. Effect of tuned mass damper on displacement demand of base-isolated structures. Engineering Structures. 2008;30:3478-88. https://doi.org/10.1016/j.engstruct.2008.05.027

[8] Hessabi RM, Mercan O, Ozturk B. Exploring the effects of tuned mass dampers on the seismic performance of structures with nonlinear base isolation systems. Earthquakes and Structures. 2017;12:285-96. https://doi.org/10.12989/eas.2017.12.3.285

[9] Shoaei P, Oromi HT. A combined control strategy using tuned liquid dampers to reduce displacement demands of base-isolated structures: a probabilistic approach. Frontiers of Structural and Civil Engineering. 2019;13:890-903. https://doi.org/10.1007/s11709-019-0524-8

[10] Love JS, Tait MJ, Toopchi-Nezhad H. A hybrid structural control system using a tuned liquid damper to reduce the wind induced motion of a base isolated structure. Engineering Structures. 2011;33:738-46. https://doi.org/10.1016/j.engstruct.2010.11.027

[11] Adam C, Di Matteo A, Furtmuller T, Pirrotta A. Earthquake excited base-isolated structures protected by tuned liquid column dampers: design approach and experimental verification. In: Vestroni F, Romeo F, Gattulli V, editors. X International Conference on Structural Dynamics. Amsterdam: Elsevier Science Bv; 2017. p. 1574-9.

[12] Furtmuller T, Di Matteo A, Adam C, Pirrotta A. Base-isolated structure equipped with tuned liquid column damper: An experimental study. Mechanical Systems and Signal Processing. 2019;116:816-31. https://doi.org/10.1016/j.ymssp.2018.06.048

[13] Masnata C, Di Matteo A, Adam C, Pirrotta A. Smart structures through nontraditional design of Tuned Mass Damper Inerter for higher control of base isolated systems. Mechanics Research Communications. 2020;105:103513. https://doi.org/10.1016/j.mechrescom.2020.103513

[14] Kawamata S. Development of a vibration control system of structures by means of mass pumps. Tokyo, Japan: Institute of Industrial Science, University of Tokyo; 1973.

[15] Ikago K, Sugimura Y, Saito K, Inoue N. Optimum seismic response control of multiple degree of freedom structures using tuned viscous mass dampers. Proceedings of the Tenth International Conference on Computational Structures Technology. Valencia, Spain2010.

[16] Ikago K, Saito K, Inoue N. Seismic control of single-degree-of-freedom structure using tuned viscous mass damper. Earthquake Engineering and Structural Dynamics. 2012;41. https://doi.org/10.1002/eqe.1138

[17] Nakamura Y, Hanzawa T, Isoda K. Performance-based placement design of tuned inertial mass dampers.2013.

[18] Ikago K, Sugimura Y, Saito K, Inoue N. modal response characteristics of a multiple-degree-of-freedom structure incorporated with tuned viscous mass dampers. Journal of Asian Architecture and Building Engineering. 2012;11:375-82. https://doi.org/10.3130/jaabe.11.375

[19] Wang FC, Hong MF, Lin TC. Designing and testing a hydraulic inerter. Journal of Mechanical Engineering Science. 2011;225:66-72. https://doi.org/10.1243/09544062jmes2199

[20] Chen L, Ren H, Wang R, Sun Z, Chen B. Simulations and tests for mechanical properties of a hydraulic inerter. Journal of Vibration and Shock. 2014;33:87-92.

[21] De Domenico D, Ricciardi G, Zhang R. Optimal design and seismic performance of tuned fluid inerter applied

to structures with friction pendulum isolators. Soil Dynamics and Earthquake Engineering. 2020;132. https://doi.org/10.1016/j.soildyn.2020.106099

[22] Saitoh M. On the performance of gyro-mass devices for displacement mitigation in base isolation systems. Structural Control and Health Monitoring. 2012;19:246-59. https://doi.org/10.1002/stc.419

[23] Asai T, Araki Y, Ikago K. Structural control with tuned inertial mass electromagnetic transducers. Structural Control and Health Monitoring. 2017;25:e2059. https://doi.org/10.1002/stc.2059

[24] De Domenico D, Ricciardi G, Zhang R. Optimal design and seismic performance of tuned fluid inerter applied to structures with friction pendulum isolators. Soil Dynamics and Earthquake Engineering. 2020;132:106099. https://doi.org/10.1016/j.soildyn.2020.106099

[25] Sugimura Y, Goto W, Tanizawa H, Nagasaku T, Saito K, Ninomiya T et al. Response control effect of high-rised steel building structure using tuned viscous mass dampers. Journal of Technology and Design. 2012;18:441-6. https://doi.org/10.3130/aijt.18.441

[26] Saito K, Sugimura Y, Inoue N. A study on response control of a structure using viscous damper with inertial mass. Journal of Structural Engineering 2008;B54:635-48.

[27] Arai T, Aburakawa T, Ikago K, Hori N, Inoue N. Verification on effectiveness of a tuned viscous mass damper and its applicability to non-linear structural systems. Journal of Structural and Construction Engineering 2009;74:1993-2002. https://doi.org/10.3130/aijs.74.1993

[28] Zhang RF, Zhao ZP, Pan C, Ikago K, Xue ST. Damping enhancement principle of inerter system. Structural Control and Health Monitoring. 2020. https://doi.org/10.1002/stc.2523

[29] Saito K, Yogo K, Sugimura Y, Nakaminami S, Park K. Application of rotary inertia to displacement reduction for vibration control system. 2004.

[30] Jiang YY, Zhao ZP, Zhang RF, De Domenico D, Pan C. Optimal design based on analytical solution for storage tank with inerter isolation system. Soil Dynamics and Earthquake Engineering. 2020;129:10. https://doi.org/10.1016/j.soildyn.2019.105924

[31] Zhao ZP, Zhang RF, Jiang YY, Pan C. Seismic response mitigation of structures with a friction pendulum inerter system. Engineering Structures. 2019;193:110-20. https://doi.org/10.1016/j.engstruct.2019.05.024

[32] Zhang RF. Seismic response control of liquid storage tanks. Shanghai: Tongji university. 2014.

[33] Zhang RF, Zhao ZP, Pan C. Influence of mechanical layout of inerter systems on seismic mitigation of storage tanks. Soil Dynamics and Earthquake Engineering. 2018;114:639-49. https://doi.org/10.1016/j.soildyn.2018.07.036

[34] De Domenico D, Impollonia N, Ricciardi G. Soil-dependent optimum design of a new passive vibration control system combining seismic base isolation with tuned inerter damper. Soil Dynamics and Earthquake Engineering. 2018;105:37-53. https://doi.org/10.1016/j.soildyn.2017.11.023

[35] Qian F, Luo YF, Sun HX, Tai WC, Zuo L. Optimal tuned inerter dampers for performance enhancement of vibration isolation. Engineering Structures. 2019;198:14. https://doi.org/10.1016/j.engstruct.2019.109464

[36] Li L, Liang Q. Effect of inerter for seismic mitigation comparing with base isolation. Structural Control and Health Monitoring. 2019;26. https://doi.org/10.1002/stc.2409

[37] De Domenico D, Ricciardi G. Improving the dynamic performance of base-isolated structures via tuned mass damper and inerter devices: A comparative study. Structural Control and Health Monitoring. 2018;25:24. https://doi.org/10.1002/stc.2234

[38] Di Matteo A, Masnata C, Pirrotta A. Simplified analytical solution for the optimal design of tuned mass damper inerter for base isolated structures. Mechanical Systems and Signal Processing. 2019;134:13. https://doi.org/10.1016/j.ymssp.2019.106337

[39] Masnata C, Di Matteo A, Adam C, Pirrotta A. Assessment of the tuned mass damper inerter for seismic response control of base-isolated structures. Structural Control and Health Monitoring. 2020. https://doi.org/10.1002/stc.2665

[40] De Angelis M, Giaralis A, Petrini F, Pietrosanti D. Optimal tuning and assessment of inertial dampers with grounded inerter for vibration control of seismically excited base-isolated systems. Engineering Structures. 2019;196:19. https://doi.org/10.1016/j.engstruct.2019.05.091

[41] Zhao ZP, Zhang RF, Wierschem NE, Jiang YY, Pan C. Displacement mitigation-oriented design and mechanism for inerter-based isolation system. Journal of Vibration and Control. 2020. https://doi.org/10.1177/1077546320951662

[42] Pan C, Zhang RF. Design of structure with inerter system based on stochastic response mitigation ratio. Structural Control and Health Monitoring. 2018;25:e2169. https://doi.org/10.1002/stc.2169

[43] Ogino M, Sumiyama T. Structural Design of a high-rise building using tuned viscous mass dampers installed across three consecutive storeys. Proceedings of the 12th International Conference on Computational Structures Technology. Stirlingshire Scotland: Civil-Comp Press; 2014.

[44] Shi X, Zhu S. A comparative study of vibration isolation performance using negative stiffness and inerter dampers. Journal of the Franklin Institute-Engineering and Applied Mathematics. 2019;356:7922-46. https://doi.org/10.1016/j.jfranklin.2019.02.040

[45] Zhao ZP, Chen QJ, Zhang RF, Jiang YY, Pan C. A negative stiffness inerter system (NSIS) for earthquake protection purposes. Smart Structures and Systems. 2020;26:481-93. https://doi.org/10.12989/sss.2020.26.4.481

[46] Wang X, He T, Shen Y, Shan Y, Liu X. Parameters optimization and performance evaluation for the novel inerter-based dynamic vibration absorbers with negative stiffness. Journal of Sound and Vibration. 2019;463:114941. https://doi.org/10.1016/j.jsv.2019.114941

[47] Crandall SH, Mark WD. Random vibration in mechanical systems [M]. London: Academic Press; 2014.

[48] Newton GC. Analytical Design of Linear Feedback Controls. United States: John Wiley & Sons, Inc; 1957.

[49] Man FCFC, D DK, N KP. Advanced Mathematics for Engineering and Science: World Scientific.

[50] Chopra AK. Dynamics of structures: theory and applications to earthquake engineering. Fourth Edition. New York: Prentice Hall. 2012.

[51] Hu LX. Earthquake Engineering. Second Edition. China: Beijing. 2006.

[52] Chinese Code for Seismic Design of Buildings (GB50011-2010). Beijing, China: China architecture and building Press; 2010.

[53] Nakaminami S, Ikago K, Inoue N, Kida H. Response characteristics of a base-isolated structure incorporated with a force-restricted viscous damper. The 15th World Conference on Earthquake Engineering. Lisbon Portugal. 2012.

[54] Naeim F. Earthquake engineering—from engineering seismology to performance-based engineering. Earthquake Spectra. 2005;21. https://doi.org/10.1193/1.1896960

[55] Atik L, Abrahamson N. An improved method for nonstationary spectral matching. Earthquake Spectra. 2010;26. https://doi.org/10.1193/1.3459159

[56] Pan C, Zhang RF. EQSignal: A useful tool to process and generate earthquake signals. 2016.

[57] Pan C, Zhang RF, Luo H, Shen H. Target-based algorithm for baseline correction of inconsistent vibration signals. Journal of Vibration and Control. 2018;24:2562–75. https://doi.org/10.1177/1077546316689014

[58] Ancheta T D, Darragh R B, P SJ. Pacific Earthquake Engineering Research Center (PEER). 2013.

Tables

TABLE 1 Benchmark model information [53]

Story number	Original structure			Equivalent SDOF model		
	Height (m)	Mass (kg)	Stiffness (kN/m)	Height (m)	Mass (kg)	Stiffness (kN/m)
7	4.70	1039000	1475900			
6	3.80	3897000	3143400			
5	3.80	3477000	4581300			
4	3.80	3600000	4976600	4.14	21015000	1195770
3	4.40	3615000	3877500			
2	4.40	3856000	4075700			
1	5.45	4671000	3519300			

TABLE 2 Optimum parameter results

Control case	Parameters	value
Isolated structure with the inerter system	K_h (kN/m)	132237
	μ	0.108
	m_{in} (kg)	2930000
	ξ	0.013
	c_d (kN·s/m)	1591
	κ	0.121
	k_d (kN/m)	16010

TABLE 3 Natural seismic waves for time history analysis

Earthquake event	Year	Recording station	Richter magnitude	ID
Imperial Valley	1940	El Centro Array	6.95	NW1
Northern California	1941	Ferndale City Hall	6.4	NW2
Parkfield	1966	Cholame Shandon Array	6.19	NW3
Borrego Mtn	1968	El Centro Array	6.63	NW4
San Fernando	1971	Palmdale Fire Station	6.61	NW5

TABLE 4 Performance indicators of isolated structure with the inerter system

Input excitations	β_h	u_{iso} (mm)
AW1	0.344	365.9
AW2	0.342	377.0
NW1	0.367	353.9
NW2	0.361	381.1

NW3	0.344	302.8
NW4	0.406	389.9
NW5	0.363	320.5
Average value	0.361<0.4	355.9<360

Appendix

Practical iteration method for solving monotone function

Here, the detail iterative process of calculating the target equivalent damping ratio $\zeta_{eq,t}$ and the inertance-mass ratio μ of the isolated structure with the inerter system is presented.

From the seismic influence coefficient specified in the seismic design code [52], the design spectrum can be expressed as follows

$$S_a = \begin{cases} \left[(10\eta_2 - 4.5)T\alpha_{\max} + 0.45\alpha_{\max}\right]g & 0 < T \le 0.1 \\ \eta_2\alpha_{\max}g & 0.1 < T \le T_g \\ (T_g/T)^{\gamma}\eta_2\alpha_{\max}g & T_g < T \le 5T_g \\ \left[\eta_2 0.2^{\gamma} - \eta_1(T - 5T_g)\right]\alpha_{\max}g & 5T_g < T \le 6 \end{cases} \tag{1}$$

where T is the natural period of the primary structure; T_g is the characteristic period of the site; $\alpha_{\max}$ is maximum seismic influence coefficient; η_1 is the slope adjustment coefficient; η_2 is the damping adjustment coefficient and g is the gravitational acceleration. It can be seen that the seismic action mitigation ratio β_h decreases with the increase of $\zeta_{eq,t}$ based on the equation list below

$$\beta_h = \frac{F}{F_0} = \frac{S_a\left(T_b, \zeta_{eq,t}\right)}{\chi S_a\left(T_0, \zeta\right)} \tag{2}$$

Therefore, the solution of Equation (2) can be simplified via numerical iteration as follows: choosing an initial equivalent damping ratio $\zeta_{eq}^{(0)}$ first, then calculate the corresponding $\beta_h^{(0)}$

$$\beta_h^{(0)} = \frac{S_a\left(T_b, \zeta_{eq}^{(0)}\right)}{\chi S_a\left(T_0, \zeta\right)} \tag{3}$$

If $\beta_h^{(0)} \neq \beta_h$, recalculate the next-step equivalent damping ratio $\zeta_{eq}^{(1)}$ via the convergence equation

$$\zeta_{eq}^{(1)} = \left(\frac{\beta_h^{(0)}}{\beta_h}\right)^{\eta} \zeta_{eq}^{(0)} \tag{4}$$

where $\eta > 1$ is an exponent to accelerate the iterative process. Then, the corresponding $\beta_h^{(1)}$ can be

calculated based on Equation (2). Repeat the above step until $\beta_h^{(n)} \approx \beta_h$, the final equivalent damping ratio $\zeta_{eq,t}$ thus can be obtained: $\zeta_{eq,t} = \zeta_{eq}^{(n)}$.

Based on the obtained $\zeta_{eq,t}$ above, the inertance-mass ratio μ can also be obtained using the same method. From the main body of the paper can be known

$$\zeta_{eq} = \alpha^2 \xi = \frac{1}{3-\mu}\sqrt{\frac{\mu}{2(1-\mu)}} \tag{5}$$

The first-order derivative of ζ_{eq} with respect to μ can be obtained

$$\frac{d\zeta_{eq}}{d\mu} = \frac{1}{(3-\mu)^2}\sqrt{\frac{\mu}{2(1-\mu)}} + \left[\sqrt{\frac{1}{\mu(1-\mu)}} + \sqrt{\frac{\mu}{(1-\mu)^3}}\right]\frac{1}{2\sqrt{2}(3-\mu)} \tag{6}$$

On account of $0 \le \mu \le 1$, Equation (6) is a monotone function which μ can be obtained through easy iteration based on the same principle discussed above. Choose an initial $\mu^{(0)}$ first, then calculate the corresponding $\zeta_{eq}^{(0)}$ based on Equation (5)

$$\zeta_{eq}^{(0)} = \frac{1}{3-\mu^{(0)}}\sqrt{\frac{\mu^{(0)}}{2\left(1-\mu^{(0)}\right)}} \tag{7}$$

If $\zeta_{eq}^{(0)} \neq \zeta_{eq,t}$, recalculate the next-step $\mu^{(1)}$ via the convergence equation

$$\mu^{(1)} = \left(\frac{\zeta_{eq,t}}{\zeta_{eq}^{(0)}}\right)^{\eta} \mu^{(0)} \tag{8}$$

Then, the corresponding $\zeta_{eq}^{(1)}$ can be calculated based on Equation (5). Repeat the above step until $\zeta_{eq}^{(n)} \approx \zeta_{eq,t}$, the final equivalent damping ratio μ thus can be obtained: $\mu = \mu^{(n)}$.

Derivation process of the seismic action ratio χ

Here, the specific derivation process of seismic action ratio χ in Equation (36) is presented.

According to the mode-superposition response spectrum method, the seismic action of each story in the multi-story structure under a particular mode can be calculated as follows [50]

$$F_{ji} = \alpha_j \gamma_j X_{ji} G_i \tag{9}$$

in which the subscript i and j denote the i-th story and the j-th mode, respectively; α is the seismic

influence coefficient [52]; X is the inter-story relative displacement; G is the gravity load of each story; γ is the modal participation factor, which can be expressed as follow [50]

$$\gamma_j = \sum_{i=1}^{n} X_{ji} G_i \Big/ \sum_{i=1}^{n} X_{ji}^2 G_i \tag{10}$$

Then the structural seismic action F_j corresponding to j-th mode can be obtained

$$F_j = \sum_{i=1}^{n} F_{ji} = \alpha_j \gamma_j \sum_{i=1}^{n} X_{ji} G_i \tag{11}$$

Assuming the original structure is within linear elastic state, the seismic action of the original multi-story structure (without additional isolation system) can be expressed as follows

$$F_0 = \chi M_0 S_a (T_0, \zeta) \tag{12}$$

where T_0 is the natural period of the original structure, and χ is the seismic action ratio of the original multi-story structure to the equivalent SDOF structure, which can be expressed as follows

$$\chi = \frac{F_0}{M_0 S_a (T_0, \zeta)} = \frac{F_0}{\eta_j \sum_{i=1}^{n} G_i} \tag{13}$$

Assuming that the gravity load and height of each story are the same, substituting Equation (10) and (11) into Equation (13) yields that

$$\chi = \frac{(\sum_{i=1}^{n} X_{ji})^2}{(N \sum_{i=1}^{n} X_{ji}^2)} \tag{14}$$

where N is the story of the original structure. Based on the assumption illustrated in Section 4.1 (the original structure is within linear elastic state), Equation (14) can be further expressed as

$$\chi \approx \frac{3(N+1)}{2(2N+1)} \tag{15}$$